

ARTICLE OPEN



Reconfigurable continuously-coupled 3D photonic circuit for Boson Sampling experiments

Francesco Hoch^{1,5}, Simone Piacentini^{2,3,5}, Taira Giordani¹, Zhen-Nan Tian^{3,4}, Mariagrazia Iuliano¹, Chiara Esposito¹, Anita Camillini¹, Gonzalo Carvacho¹, Francesco Ceccarelli³, Nicolò Spagnolo¹, Andrea Crespi^{2,3}, Fabio Sciarrino¹✉ and Roberto Osellame³✉

Boson Sampling is a computational paradigm representing one of the most viable and pursued approaches to demonstrate the regime of quantum advantage. Recent results have shown significant technological leaps in single-photon generation and detection, leading to progressively larger instances of Boson Sampling experiments in different photonic systems. However, a crucial requirement for a fully-fledged platform solving this problem is the capability of implementing large-scale interferometers, that must simultaneously exhibit low losses, high degree of reconfigurability and the realization of arbitrary transformations. In this work, we move a step forward in this direction by demonstrating the adoption of a compact and reconfigurable 3D-integrated platform for photonic Boson Sampling. We perform 3- and 4-photon experiments by using such platform, showing the possibility of programming the circuit to implement a large number of unitary transformations. These results show that such compact and highly-reconfigurable layout can be scaled up to experiments with larger number of photons and modes, and can provide a viable direction for hybrid computing with photonic processors.

npj Quantum Information (2022)8:55; <https://doi.org/10.1038/s41534-022-00568-6>

Since the original proposal of a computational paradigm based on the rules of quantum mechanics¹, large research efforts have been devoted to identifying the optimal approach to implement a universal quantum computer^{2,3}. Besides the great promises provided by such computational paradigm, the implementation of a large-scale universal quantum device capable to outperform or, at least, to be comparable with a classical computer is still a challenging task. In view of the very recent advances in quantum technologies, approaching the noisy intermediate-scale quantum (NISQ) era, the current target is to reach a fundamental milestone named quantum computational advantage. The goal is to achieve, unambiguously and possibly with different platforms and approaches, the scenario where a quantum device is capable of solving a specific task faster than any classical counterpart.

Among the several quantum algorithms that provide a computational speed-up, two strategies emerge as the most suitable for their experimental realizations⁴. The first one requires to sample the output states produced by a random quantum circuit. This paradigm has been recently implemented in quantum processors based on superconducting qubits^{5,6}. The second approach is based on a different albeit related task, named Boson Sampling (BS)^{7,8}, which requires sampling from the distribution of non-interacting bosons scattered by a random unitary transformation. Here, the hardness of simulating such a bosonic system is strictly connected to quantum interference effects due only to particle indistinguishability⁹. Classical simulation of Boson Sampling, even approximately, is computationally-hard since it requires calculation of permanents of complex-entrined matrices, a #P-hard problem. A natural way to reproduce this dynamics and sampling effectively from the output distribution of such process can be obtained via a photonic quantum processor. Reaching the

quantum advantage regime with this approach requires the generation of a set of n highly-indistinguishable single photons, which evolve via quantum interference in a low-loss linear optical network with $m \sim n^2$ modes capable of implementing a random transformation according to the Haar measure (see Fig. 1a). Samples are then collected by direct measurement of the output modes. In this direction, several proof-of-principle implementations have been reported exploiting photonic platforms^{10–19}, including one of the latest experiments with the detection of 14 photons after propagation in an interferometer with 60 ports²⁰.

Starting from these results, research efforts have been dedicated to technological advances enabling to enlarge the dimensionality of photonic processors, and to theoretical investigations^{21,22} aimed at a precise definition of the limits of a classical simulation of Boson Sampling with experimental imperfections. In parallel, the Boson Sampling paradigm has triggered the definition of a set of variants of the original formulation with the aim of improving the efficiency of the corresponding photonic platform while preserving the classical computational complexity of the task. Examples include (but are not limited to) Scattershot Boson Sampling (SBS)²³ and Gaussian Boson Sampling (GBS)²⁴. SBS exploits probabilistic parametric down-conversion sources placed at each input mode of the interferometer in a heralded configuration (see Fig. 1b), leading to an exponential growth in the samples acquisition^{18,25,26}. In the GBS paradigm^{26–28}, Fock states are replaced by single-mode squeezed vacuum states (see Fig. 1c). By using the GBS approach, recent experiments have reported the achievement of quantum advantage with a photonic platform^{29,30}. Furthermore, GBS has been recently pointed out to have potential application for hybrid classical-quantum computing, due to the connection with other

¹Dipartimento di Fisica, Sapienza Università di Roma, Piazzale Aldo Moro 5, I-00185 Roma, Italy. ²Dipartimento di Fisica, Politecnico di Milano, Piazza Leonardo da Vinci, 32, I-20133 Milano, Italy. ³Istituto di Fotonica e Nanotecnologie, Consiglio Nazionale delle Ricerche (IFN-CNR), Piazza Leonardo da Vinci, 32, I-20133 Milano, Italy. ⁴State Key Laboratory of Integrated Optoelectronics, College of Electronic Science and Engineering, Jilin University, 130012 Changchun, China. ⁵These authors contributed equally: Francesco Hoch, Simone Piacentini. ✉email: fabio.sciarrino@uniroma1.it; roberto.osellame@cnr.it

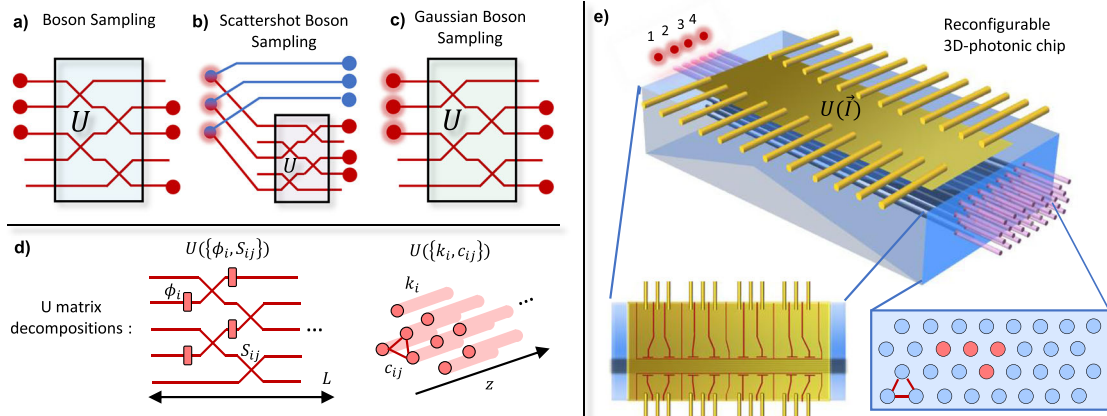


Fig. 1 Boson Sampling in a 3D continuous-coupling integrated device. **a** Boson Sampling (BS) and the most recent variants, **(b)** Scattershot Boson Sampling (SBS) and **(c)** Gaussian Boson Sampling (GBS). The corresponding computational problems require sampling from the output distribution using different input quantum states of light, such as Fock states in BS, two-mode squeezed vacuum states in SBS and single-mode squeezed vacuum states in GBS. The common element among the schemes is the optical random circuit, described by the unitary evolution U . **d** The most widely adopted decomposition of the operator U is via a network of beamsplitters, with splitting ratios S_{ij} and phase-shifts ϕ_i (left); an alternative implementation exploits continuous-coupling by evanescent waves among waveguides (right) depending on the coupling coefficients c_{ij} and the propagation constants k_i , where both may vary along the direction z . **e** Overview of the reconfigurable 3D integrated photonic chip, realized through the femtosecond laser writing technique. The device is composed by 32 optical-modes arranged in a triangular lattice, as showed in the inset reporting the transverse section of the sample. In red we have highlighted the input modes employed in the 3- and 4-photon experiment. The transformation U is controlled by the 16 resistors fabricated on top of the glass sample. The second inset shows the top view of the electrical circuits that controls the currents I_i applied to the resistors.

problems including graph theory^{31,32} or simulation of molecular vibronic spectra^{33,34}. In all previous experiments reporting Boson Sampling instances, including its variants, different platforms have been employed to realize linear optical transformations. However, all the requirements for a fully-developed processor, namely low-loss, reconfigurability, and the possibility to implement random transformations, are currently not fulfilled simultaneously in a single system. Indeed, low-loss systems are necessary to avoid spoiling the complexity of the process^{35,36}, and full-reconfigurability is a crucial requirement on two main aspects. On one side, such a feature is essential to benchmark the effective Haar-randomness of the platform, which is at the basis of complexity conjectures^{7,37}. On the other side, reconfigurability is needed to achieve programmable processors for applications beyond the quantum advantage demonstration²⁸. With current-up-to-date experiments, low-loss platforms lack an active reconfiguration capability to change the transformation implemented by the optical circuit^{20,29,30} and their capability of Haar-random operations has not been demonstrated yet. Conversely, integrated photonic architectures based on universal decompositions^{38,39} permit full reconfiguration capabilities, but still require further technological improvements also in terms of loss-reduction to scale up the number of modes.

Here, we perform a step forward towards developing a photonic platform encompassing all the aforementioned characteristics. We report the realization of a photonic reconfigurable integrated device with a compact structure. Such device provides significant advantages in terms of losses and number of modes. In addition, it possesses a high degree of reconfigurability enabling the implementation of a large number of transformations, in contrast to previous works that implement static integrated circuits via the same technology^{19,40}. This architecture takes advantage from the 3D-capability of the femtosecond laser-writing technique of waveguides in glass^{41,42}. The optical circuit is realized via continuous-coupling of 32 waveguides arranged in a triangular lattice. The device is then controlled by changing the currents applied to the 16 heaters fabricated on top of the interferometer. We show the reconfiguration capabilities of the device by providing a thorough analysis on the set of unitary

transformations which can be reached by the system. Then, we benchmark our platform in the Boson Sampling scenario by performing and validating 3-photon and 4-photon experiments with several different configurations of the optical transformation.

RESULTS

Reconfigurable integrated 3D photonic chip

Integrated photonics has demonstrated significant advances in realizing complex optical circuits for quantum information processing⁴². Nowadays integrated optical circuits are the most promising photonic platforms to implement large-scale interferometer with high-level of reconfigurability. The unitary operations that describe a given optical circuit are often decomposed in elementary optical units. The scheme by Reck et al.³⁸ decomposes an optical circuit with m optical modes in the product of $m(m-1)/2$ two-mode beamsplitters and single-mode phase-shifters. A more recent algorithm by Clements et al.³⁹ optimizes the arrangement of the optical elements to minimize the sensitivity to fabrication imperfections and to photon losses. In this framework, any unitary transformation is determined by the set of phases ϕ_i and splitting ratios S_{ij} in the circuit (see Fig. 1d). In reconfigurable integrated circuit, heaters placed in correspondence to the waveguide enable to change locally the refractive index of the material thus inducing a change in the relative phases among the optical modes. Despite the aforementioned schemes have been adopted in several experiments^{12,28,43–46}, scaling the circuit to large number of modes is a challenging task in terms of size of the device, related to the amount of losses and to the number of required optical elements. In Fig. 1d we depict the approach that we employ in this paper, which is different with respect to the traditional decomposition of unitaries in beamsplitters and phase-shifters. Such a scheme exploits the continuous coupling of the radiation in waveguides arrays. In this framework it is possible to associate a Hamiltonian $\mathcal{H}(z)$ to the system given the coupling coefficients $c_{ij}(z)$ between neighbouring modes and the propagation constants of the modes $k_i(z)$. Coupling coefficients and propagation constants may change along the propagation coordinate z . The unitary transformation of the

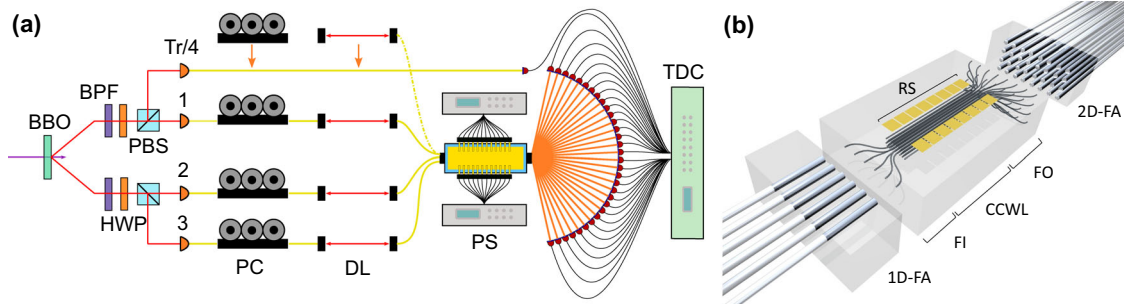


Fig. 2 **Scheme of the experimental apparatus.** **a** A parametric down-conversion process in a Beta-Barium Borate crystal generates one- and two-pair photon states. Generation in the single-pair regime is employed for the unitary reconstruction procedures, while 3- and 4-photon states are employed for experiments in the Boson Sampling framework. Photons are prepared in their polarization and temporal degrees of freedom before coupling in the input single-mode fiber array. After evolution, photons are finally detected via a set of 32 single-photon avalanche photodiodes connected to a 32-channel time-to-digital converter for the reconstruction of the coincidence pattern. **b** Schematic of the in- and out-coupling of the single photons with the 3D photonic circuit: one- and two-dimensional fiber arrays connect to the fan-in and fan-out sections of the circuit. Legend: BBO beta-barium borate crystal, BPF band-pass filter, HWP half-wave plate, PBS polarizing beamsplitter, PC polarization controller, DL delay line, PS power supply, TDC time-to-digital converter, 1D-/2D-FA one-/two-dimensional fiber array, FI fan-in, FO fan-out, CCWL continuously-coupled waveguide lattice, RS resistors.

circuit can be obtained by integrating $\mathcal{H}(z)$ for the whole length of the interaction region, which maps the time evolution of the system. In particular, in our case we employ a three-dimensional array, in which waveguides are arranged according to a triangular-lattice cross-section. Such architecture offers practical advantages in terms of compactness, losses and circuit length in comparison to other approaches. Exemplarily, it is striking to note that in this work we have achieved reconfigurable 32-modes random unitaries in a 7.5-cm long optical chip, while a reconfigurable discretely-coupled interferometer with the same number of modes and produced with the same technology would have required a device length of about 30 cm. Such aspects are widely discussed in Supplementary Note 1. In detail, our integrated device, depicted in Fig. 1e, comprises 32 continuously-coupled single-mode waveguides in a 8×4 arrangement, fabricated by femtosecond laser direct writing in a borosilicate glass substrate^{41,47}. The waveguide positions are randomly modulated along the propagation coordinate z with respect to the positions of a regular triangular lattice. These modulations introduce randomness in the c_{ij} coefficients and thus in the circuit transformation, which otherwise would be highly symmetric and not suitable for a Boson Sampling experiment. To add circuit reconfigurability, 16 resistive heaters have been patterned, by femtosecond laser ablation, on a gold film deposited on the substrate surface. The resistors are equally distributed on the two sides of the interaction region. An external power supply controls the currents applied to the resistors. Dissipated power in this process induces thermal gradients in the substrate and thus locally changes the refractive index of the waveguides^{48,49}. This modulates the propagation constants k_i of the waveguides by the thermo-optic effect, thus allowing to change dynamically the transformation U implemented in the integrated device. Hence, we demonstrate that the thermo-optic phase-shifting technology can also be applied to three-dimensional, continuously-coupled waveguide devices. Additional details on the circuit geometry and on the fabrication process are provided in the Methods section.

Experimental platform

Let us now illustrate the components of the experimental platform employed to benchmark the photonic device and to collect the 3- and 4-photon samples (see Fig. 2a). We exploit one- and two-pair emission in a type-II spontaneous parametric down-conversion source composed of a beta-barium borate crystal operating at 785 nm. The first stage of the apparatus includes all the optical components to generate the state resource to perform sampling with either indistinguishable and distinguishable photons.

Photons spectra are filtered through a 3 nm band-pass filter. Then, photons are split in four different spatial modes according to the polarization via half-wave plates and polarizing beamsplitters, and coupled into single-mode fibers. Photons are controlled in polarization and in time-of-arrival by polarization controllers and delay lines respectively, in order to tune their degree of indistinguishability. Then, they are injected into the reconfigurable integrated chip via an array of 6 single-mode fibers that has been aligned and glued to the device. A fan-in waveguide section leads the photons to selected inputs of the waveguide array (see Fig. 2b). After the evolution in the integrated device, a fan-out waveguide section leads the photons to a 8×4 rectangular multimode fiber array that matches the fan-out geometry. It is worth noting that the 2D fiber array further helps the compactness of the device by greatly reducing the length of the fan-out section (see Supplementary Note 1 and Supplementary Figs. 1–2). The detection stage includes 32 single-photon avalanche photodiodes. We have developed a custom software that simultaneously controls the delay lines, the power supply and the 32-channel time-to-digital converter module to record two- and four-fold coincidences. This implies a full control over the unitary transformation implemented in the circuit, the switching between indistinguishable and distinguishable photons, and the recording and processing of the data samples.

Unitary matrix sampling and reconstruction

Control over the unitary transformations implemented in the chip is performed by tuning the currents in the resistors. To verify the classes of matrices U that can be implemented by the device due to its reconfigurability, we have reconstructed a large number of different evolutions, each corresponding to a different setting for the currents in the resistors. Thus, a crucial ingredient was the adoption of a fast and efficient reconstruction algorithm. Additionally, an efficient and fast reconstruction of the unitary transformations is a fundamental step also for benchmarking and validating the 3- and 4-photon experiments described in the next section. We made use of an adapted version of the method reported in⁵⁰ (see Supplementary Note 2 and Supplementary Fig. 3). The latter envisages the measurements of two-photon Hong-Ou-Mandel (HOM) dips resulting from pairs of photons injected in different combinations of input ports. In our case we restricted the measurements to two of the possible input pair combinations for the reconstruction of 3×32 sub-matrices and to only three pairs in the case of 4×32 sub-matrices. From each input pair we analysed 496 HOM dips, namely all the possible non-redundant pairs obtained by the combination of the 32 output ports. From these

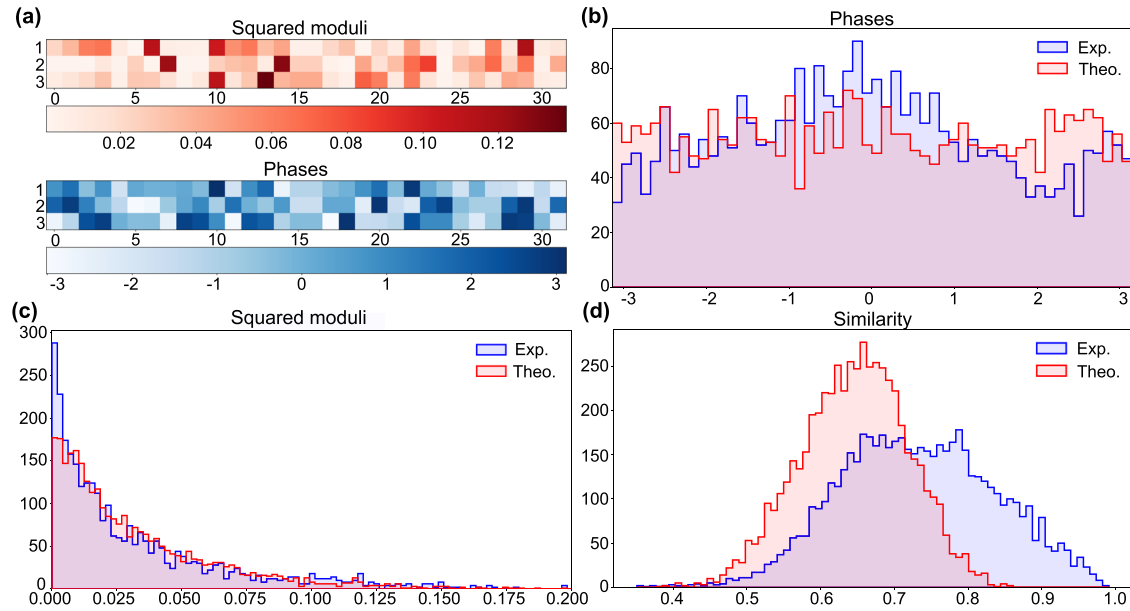


Fig. 3 Experimental reconstruction of the $[3 \times 32]$ sub-matrices and comparison with the Haar-random matrices. **a** Experimental reconstruction of the squared moduli ρ_{ij}^2 (red) and phases θ_{ij} (blue) for three input ports of the reconfigurable photonic chip, highlighted by the labels in the figure. The chip is set on a random configuration of currents. Each input port represents a row of the unitary transformation applied to the input state. **b**, **c** Comparison of the phases and the squared moduli frequency distribution respectively, between 15 experimentally reconstructed sub-matrices (blue) and 15 $[3 \times 32]$ sub-matrices sampled from the Haar-random unitaries (red). **d** Distribution of the similarity between the squared moduli of two columns of different sub-matrices. We repeated the measurement for ~ 200 different configurations of the currents in the chip. In red it is shown the theoretical similarity distribution obtained by sampling columns distributed according to the Haar measure. The overlap between the two histograms is the 62.4% of the total area.

measurements we have extracted the information about the moduli ρ_{ij} and the phases θ_{ij} of the sub-matrices elements expressed as $U_{ij} = \rho_{ij}e^{i\theta_{ij}}$. In Fig. 3a we have reported an example regarding the 96 squared moduli and phases of one of the 15 different 3×32 sub-matrices reconstructed in this work. Our next step was to prove that the random unitaries, sampled by changing the currents configuration in the circuit, were drawn from a distribution as close as possible to the Haar measure. This requirement is fundamental to ensure the hardness of BS. To this aim we compared the distributions of phases and moduli of the 15 sub-matrices measured in the experiment with the one retrieved from likewise Haar-random extracted unitary matrices (Fig. 3b, c). In both cases we have obtained a good agreement between the two distributions. The slight deviations from the theoretical histograms can be explained by experimental artifacts related to losses, imperfections in the apparatus and to the algorithm for the reconstruction of the matrix. We discuss these effects in Supplementary Note 3 and Supplementary Figs. 4–6. As a final benchmark of the device, we measured 200 columns of different unitaries and calculated the similarities between the distributions given by the squared moduli of each column. The measurements were performed by sending one photon in the device and measuring it at the output in coincidence with his correlated one in a two-photon experiment. The unitaries have been generated by a uniform sampling of the electrical power dissipated in the resistors. Also in this analysis we find a good agreement with expectations, signified by the overlap with the histogram of the similarities calculated from the columns of Haar-random matrices shown in Fig. 3d. The latter result represents one of the first investigations on the level of randomness that can be reached in this continuously-coupled waveguide architecture by changing only the propagation constants via the thermo-optic effect. The similarity to the Haar-random distribution could be improved by engineering the sampling strategy of the dissipated powers, which here have been extracted from a uniform distribution. Note that, in the discrete-decomposition schemes (Reck, Clements)

there exist algorithms to set the optical circuit to sample from the Haar distribution. However, the phase shift values and beamsplitter reflectivities do not display trivial distributions^{51,52} which in turn require complex settings of the external control circuit. More precisely, by increasing the dimension of the matrix, the parameter distributions tend to be more and more peaked. For example, the uniform sampling of the dissipated electrical powers employed in this work is far from the correct sampling to generate random Haar matrices in discrete optical circuits. An exhaustive and conclusive answer regarding the possibility to extract matrices from a distribution closer to the Haar measure with a continuously-coupled waveguide architecture needs further studies both from a theoretical and experimental point of view.

Experimental Boson Sampling in a 3D reconfigurable circuit

After characterization of the device, we have then performed 3- and 4-photon experiments in the Boson Sampling framework with our integrated system. The 4-photon state from double-pair emission generated by the source can be written as $\rho^{\text{in}} \sim \alpha|1111\rangle\langle 1111| + \beta|2002\rangle\langle 2002| + \gamma|0220\rangle\langle 0220|$ (see Supplementary Note 4 and Supplementary Fig. 7), by expressing the density matrix in the occupation number of the four modes and neglecting the higher order of multi-pair emission. To inject a 3-photon $|111\rangle$ input state, one of the four output modes of the source is directly measured and thus acts as a trigger. To this end, we have discarded one output mode of the chip, due to the requirement of using one detector for the trigger photon. Four-fold coincidences between the trigger photon and three output modes are then recorded, providing the output samples. In the 4-photon experiment, we have sampled from the entire ρ^{in} by directly connecting the four output modes of the source to the integrated device (see Fig. 2). In this case, we have sampled from all the output ports of the device. For all reported experiments, our measurements are restricted to the collision-free events. Such choice does not affect significantly the outcomes of the

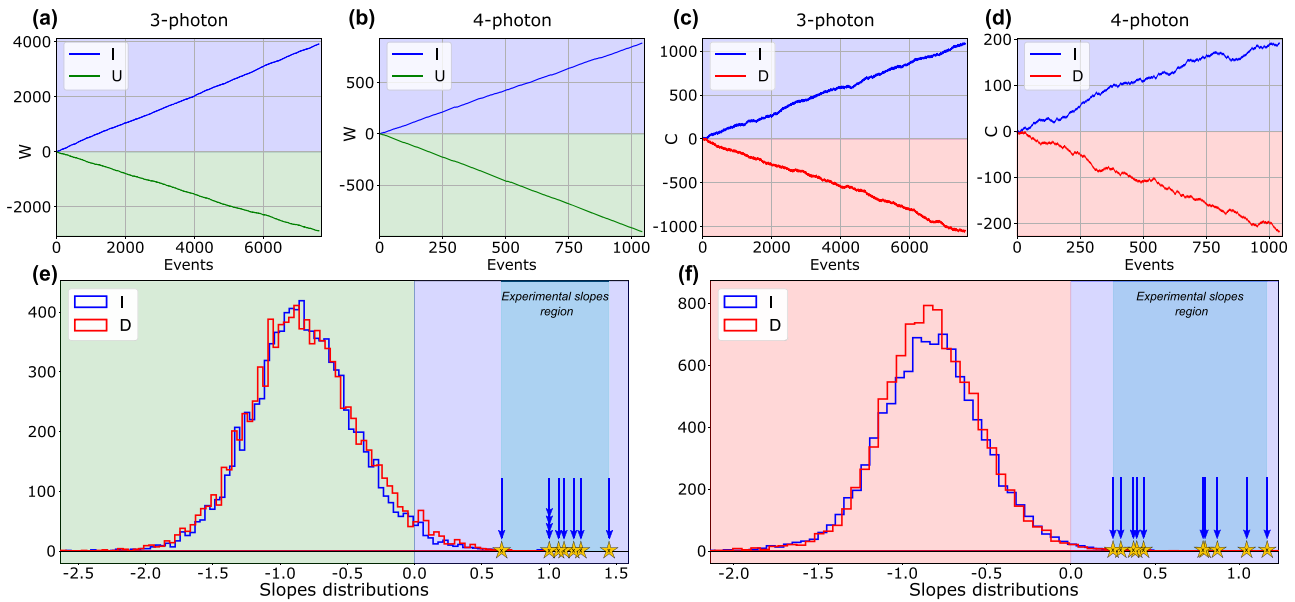


Fig. 4 Boson Sampling data. Validation of the 3-photon (blue points in (a)) and 4-photon (blue points in (b)) Boson Sampling experiments against the uniform sampler hypothesis (green point in (a), (b)). **c, d** Validation against the distinguishable photons sampler of 3- and 4-photon events. The test is applied using the same reconstructed sub-matrix in (a) and (b). The distinguishable samples (red points) were collected by adjusting the relative time delay between the input photons. **e** Histograms of simulated 3-photon slopes for counter W (normalized to the slopes of distinguishable particles data) in the case of validation against the uniform sampler using a random extracted U transformation, i.e. U matrices that do not match the actual operation implemented in the circuit. The obtained slopes of the 10 different 3-photon BS experiments are highlighted by the arrows (and by the corresponding stars). The experimental points were validated with the reconstructed sub-matrix retrieved from the two-photon reconstruction. All the experimental slopes values are in the positive range and far from the histograms average, thus showing the correct validation of the performed experiment. In (f), we performed the same analysis for the validation against the distinguishable photons hypothesis.

experiment since the configurations with more than one photon per mode display very low probabilities in the regime where the number of photons is much smaller compared to the number of the optical modes⁵³.

Let us now illustrate the analysis of the experimental samples collected in a 3- and 4-photon BS routines. In this context, the problem of data validation is pivotal to assess the correctness of the sampling process, especially in the regime in which it is not possible to reproduce the output of the experiment with classical resources. In the past years several tests have been developed to rule out classical models, such as the uniform and distinguishable particle samplers, that could reproduce some features of the BS output distribution^{54–63}. In Fig. 4 a–b we report one instance of the validation of a 3- and 4-photon BS against the uniform distribution test⁵⁴, assuming the input states described above for the two scenarios. We also employ the same data to validate the experiment against the distinguishable particles hypothesis⁵⁵ (see Fig. 4c, d, Supplementary Note 5 and Supplementary Figs. 8–11). In both tests each event collected in the experiment increases or decreases a counter, W for the case of uniform sampler and C for the distinguishable particle sampler, according to a likelihood ratio test. Positive slopes are the signatures of the successful validation of the data. These kinds of hypothesis tests require a good modelling of the system, including the knowledge of the input state and of the unitary transformation applied to the state. The latter has been reconstructed through two-photon measurements and exploiting the reconstruction algorithm discussed above (see also Supplementary Note 2). We have performed 10 different 3-photon BS experiments, and 3 different 4-photon with likewise configurations of the optical circuit. All the data were successfully validated against the two hypotheses. In Fig. 4e, f we underline the sensitivity of these validation tests to the reconstruction of the matrix representing the optical circuit. The histograms report the distribution of the slopes normalized to the one of

distinguishable particles when the unitary is chosen randomly and does not coincide with the actual transformation performed in the circuit. We note that, in absence of correspondence between the unitary transformation related to the data and the one related to the likelihood ratio computations, these tests assign the data to the negative hypothesis independently from the particle statistics. In the same figure we report the experimental slopes describing the set of 10 different 3-photon BS validated in this work using the unitary matrices reconstructed via our algorithm. The experimental points (stars in the Fig. 4e, f) are distant more than 3 standard deviations with respect to the average of the histograms, representing validations with random unitaries that do not correspond to the circuit from which the samples were generated as described above. Such additional result reinforce the successful validation of the performed experiments, and benchmark the reconstruction accuracy of the optical circuit showing a high degree of control of the platform.

DISCUSSION

In this article we have reported on the implementation and benchmarking of an integrated platform, with a compact 3D layout based on continuous waveguide coupling which includes a set of heaters to enable a high degree of reconfigurability. The employed architecture, achievable by exploiting the unique capabilities of the femtosecond laser micromachining technique, can be scaled up to larger number of modes. Indeed, we have successfully shown that our 32-mode device can implement a relevant portion of transformations according to the Haar measure, a fundamental requirement to fulfil the randomness hypothesis at the basis of the complexity of Boson Sampling. We have then implemented and validated 3- and 4-photon experiments, showing the viability of using such platform for future large-scale Boson Sampling instances. In fact, the devices

fabricated with femtosecond laser technique can be interfaced with other types of single-photon sources, such as deterministic quantum dot emitters⁶⁴. Deterministic sources are the most promising for scaling up the number of indistinguishable photons in a genuine Fock state^{65,66}. The same waveguide fabrication technology is able to realize integrated parametric sources⁶⁷ that could be included in our device to mitigate the current losses in coupling photons to single-mode fibers and at fiber-waveguide interfaces. Furthermore, the scheme with arrays of integrated sources could be feasible for realizing Scattershot and Gaussian Boson Sampling variants in a fully integrated platform^{26,28}. The capability of devising a fully-reprogrammable, large scale and compact photonic processor is fundamental also to envisage future applications beyond the original scope of the Boson Sampling. To this aim, future studies shall focus on methods that allow one to control and program the transformations that the device can implement. This means finding a model that links the parameters of the unitary transformations to the dissipated electrical powers in the heaters, which is a problem still not addressed in the literature for reconfigurable continuously-coupled waveguide circuits. We believe that the use of a black-box approach, via neural networks and optimization algorithms^{68,69}, is possible and promising. Further improvements in the reconfigurability could be brought from modifications of the present device architecture, e.g. by increasing the number of heaters and by changing their arrangement with respect to the waveguide positions.

Given the aforementioned potentiality and advantages reported in this work such a platform is expected to be at the basis of recent proposals of hybrid computing architectures^{31–34,70,71}.

METHODS

3D photonic circuit

The circuit consists of a triangular lattice with 32 continuously-coupled waveguides characterized by an average pitch of 11 μm (see Fig. 1e). Indeed, each waveguide is shifted from its standard position of a quantity randomly chosen between 0 and 2 μm along a random direction. Such shifts are varied with continuity along the whole coupling region, which is overall 36 mm long. In order to allow the coupling of single photons into the circuit, six central waveguides of the array extend through a fan-in region, rearranged in a single row with spacing of 127 μm . At the output side, a fan-out expands all the waveguides in a 8 \times 4 rectangular lattice with a pitch of 250 μm . Photons are coupled to the input of the circuit with a linear single-mode fiber array, while are collected at the output by a rectangular multimode fiber array (see Fig. 2b). Input and output fiber arrays match the geometry of the fan-in and fan-out regions, respectively. Total insertion losses are 3.5 ± 0.1 dB, depending on the input waveguide considered.

Fabrication process

The 3D photonic circuit was fabricated by femtosecond laser writing in a borosilicate glass substrate (EAGLE XG, Corning) extending on an area of 75×12 mm². The laser source (PHAROS, Light Conversion), operating at a wavelength of 1030 nm, was configured to produce pulses with duration of 170 fs and energy equal to 290 nJ at a repetition rate of 1 MHz. The laser was focused with a $20 \times$ ($NA = 0.5$) water-immersion objective, while the substrate was translated at 20 mm s⁻¹ for six consecutive scans. To ensure efficient reconfigurability, the circuit was inscribed at 30 μm from the surface. After a thermal annealing step⁷², single-mode waveguides operating at 785 nm with a $1/e^2$ mode diameter of 4.5 μm were obtained. Heaters were fabricated by depositing gold on the chip surface and patterning the electrical circuit with the process reported in⁷³. A total number of 16 resistors (length 3 mm, resistance 70 ± 13 Ω) were arranged in two parallel rows at the sides of the coupling region. To guarantee proper heat dissipation, the device was mounted on an aluminium heat sink.

DATA AVAILABILITY

The data that support the findings of this study are available from the corresponding authors upon reasonable request.

Received: 11 January 2022; Accepted: 20 April 2022;

Published online: 12 May 2022

REFERENCES

- Feynman, R. P. Simulating physics with computers. *Int. J. Theor. Phys.* **21**, 467–488 (1982).
- DiVincenzo, D. P. The physical implementation of quantum computation. *Fortschr. der Phys.* **48**, 771–783 (2000).
- Nielsen, M. A. & Chuang, I. L. *Quantum Computation and Quantum Information* (Cambridge University Press, 2010).
- Harrow, A. W. & Montanaro, A. Quantum computational supremacy. *Nature* **549**, 203 (2017).
- Arute, F. et al. Quantum supremacy using a programmable superconducting processor. *Nature* **574**, 505–510 (2019).
- Wu, Y. et al. Strong quantum computational advantage using a superconducting quantum processor. *Phys. Rev. Lett.* **127**, 180501 (2021).
- Aaronson, S. & Arkhipov, A. The computational complexity of linear optics. In *Proceedings of the 43rd annual ACM symposium on Theory of Computing*, 333–342 <https://doi.org/10.1145/1993636.1993682> (2011).
- Brod, D. J. et al. Photonic implementation of boson sampling: a review. *Adv. Photonics* **1**, 1–14 (2019).
- Hong, C. K., Ou, Z. Y. & Mandel, L. Measurement of subpicosecond time intervals between two photons by interference. *Phys. Rev. Lett.* **59**, 2044–2046 (1987).
- Broome, M. A. et al. Photonic boson sampling in a tunable circuit. *Science* **339**, 794–798 (2013).
- Spring, J. B. et al. Boson sampling on a photonic chip. *Science* **339**, 798–801 (2013).
- Crespi, A. et al. Integrated multimode interferometers with arbitrary designs for photonic boson sampling. *Nat. Photonics* **7**, 545–549 (2013).
- Tillmann, M. et al. Experimental boson sampling. *Nat. Photonics* **7**, 540–544 (2013).
- Loredo, J. C. et al. Boson sampling with single-photon fock states from a bright solid-state source. *Phys. Rev. Lett.* **118**, 130503 (2017).
- He, Y. et al. Time-bin-encoded boson sampling with a single-photon device. *Phys. Rev. Lett.* **118**, 190501 (2017).
- Wang, H. et al. High-efficiency multiphoton boson sampling. *Nat. Photonics* **11**, 361–365 (2017).
- Wang, H. et al. Toward scalable boson sampling with photon loss. *Phys. Rev. Lett.* **120**, 230502 (2018).
- Zhong, H.-S. et al. 12-photon entanglement and scalable scattershot boson sampling with optimal entangled-photon pairs from parametric down-conversion. *Phys. Rev. Lett.* **121**, 250505 (2018).
- Gao, J. et al. Experimental collision-free dominant boson sampling <https://arxiv.org/abs/1910.11320> (2019).
- Wang, H. et al. Boson sampling with 20 input photons and a 60-mode interferometer in a 10^{14} -dimensional hilbert space. *Phys. Rev. Lett.* **123**, 250503 (2019).
- Neville, A. et al. Classical boson sampling algorithms with superior performance to near-term experiments. *Nat. Phys.* **13**, 1153 (2017).
- Clifford, P. & Clifford, R. The classical complexity of boson sampling. In *Proceedings of the 2018 Annual ACM-SIAM Symposium on Discrete Algorithms (SODA)*, 146–155 <https://doi.org/10.1137/1.9781611975031.10> (2018).
- Lund, A. P. et al. Boson sampling from a gaussian state. *Phys. Rev. Lett.* **113**, 100502 (2014).
- Hamilton, C. S. et al. Gaussian boson sampling. *Phys. Rev. Lett.* **119**, 170501 (2017).
- Bentivegna, M. et al. Experimental scattershot boson sampling. *Sci. Adv.* **1** <https://advances.sciencemag.org/content/1/3/e1400255> (2015).
- Paesani, S. et al. Generation and sampling of quantum states of light in a silicon chip. *Nat. Phys.* **15**, 925–929 (2019).
- Zhong, H.-S. et al. Experimental gaussian boson sampling. *Sci. Bull.* **64**, 511–515 (2019).
- Arrazola, J. M. et al. Quantum circuits with many photons on a programmable nanophotonic chip. *Nature* **591**, 54–60 (2021).
- Zhong, H.-S. et al. Quantum computational advantage using photons. *Science* **370**, 1460–1463 (2020).
- Zhong, H.-S. et al. Phase-programmable gaussian boson sampling using stimulated squeezed light. *Phys. Rev. Lett.* **127**, 180502 (2021).
- Arrazola, J. M. & Bromley, T. R. Using gaussian boson sampling to find dense subgraphs. *Phys. Rev. Lett.* **121**, 030503 (2018).
- Schuld, M., Bradler, K., Israel, R., Su, D. & Gupt, B. Measuring the similarity of graphs with a gaussian boson sampler. *Phys. Rev. A* **101**, 032314 (2020).
- Huh, J., Guerreschi, G. G., Peropadre, B., McClean, J. R. & Aspuru-Guzik, A. Boson sampling for molecular vibronic spectra. *Nat. Photonics* **9**, 615–620 (2015).

34. Banchi, L., Fingerhuth, M., Babej, T., Ing, C. & Arrazola, J. M. Molecular docking with gaussian boson sampling. *Sci. Adv.* **6**, eaax1950 (2020).
35. Qi, H., Brod, D. J., Quesada, N. & García-Patrón, R. Regimes of classical simulability for noisy gaussian boson sampling. *Phys. Rev. Lett.* **124**, 100502 (2020).
36. García-Patrón, R., Renema, J. J. & Shchesnovich, V. Simulating boson sampling in lossy architectures. *Quantum* **3**, 169 (2019).
37. Kruse, R. et al. Detailed study of gaussian boson sampling. *Phys. Rev. A* **100**, 032326 (2019).
38. Reck, M., Zeilinger, A., Bernstein, H. J. & Bertani, P. Experimental realization of any discrete unitary operator. *Phys. Rev. Lett.* **73**, 58–61 (1994).
39. Clements, W. R., Humphreys, P. C., Metcalf, B. J., Kolthammer, W. S. & Walmsley, I. A. Optimal design for universal multiport interferometers. *Optica* **3**, 1460–1465 (2016).
40. Jiao, Z.-Q. et al. Two-dimensional quantum walk of correlated photons <https://arxiv.org/abs/2007.06554> (2020).
41. Gattass, R. R. & Mazur, E. Femtosecond laser micromachining in transparent materials. *Nat. Photonics* **2**, 219–225 (2008).
42. Wang, J., Sciarino, F., Laing, A. & Thompson, M. G. Integrated photonic quantum technologies. *Nat. Photonics* **14**, 273–284 (2020).
43. Carolan, J. et al. Universal linear optics. *Science* **349**, 711–716 (2015).
44. Harris, N. C. et al. Quantum transport simulations in a programmable nanophotonic processor. *Nat. Photonics* **11**, 447 (2017).
45. Wang, J. et al. Experimental quantum hamiltonian learning. *Nat. Phys.* **13**, 551 (2017).
46. Taballione, C. et al. 8×8 reconfigurable quantum photonic processor based on silicon nitride waveguides. *Opt. Express* **27**, 26842–26857 (2019).
47. Ariola, A. et al. Low bend loss waveguides enable compact, efficient 3d photonic chips. *Opt. Express* **21**, 2978–2986 (2013).
48. Flamini, F. et al. Thermally reconfigurable quantum photonic circuits at telecom wavelength by femtosecond laser micromachining. *Light Sci. Appl.* **4**, e354 EP – (2015).
49. Pentangelo, C., Atzeni, S., Ceccarelli, F., Osellame, R. & Crespi, A. Analytical modeling of the static and dynamic response of thermally actuated optical waveguide circuits. *Phys. Rev. Res.* **3**, 023094 (2021).
50. Laing, A. & O'Brien, J. L. Super-stable tomography of any linear optical device <https://arxiv.org/abs/1208.2868> (2012).
51. Russell, N. J., Chakhmakchyan, L., O'Brien, J. L. & Laing, A. Direct dialling of haar random unitary matrices. *N. J. Phys.* **19**, 033007 (2017).
52. Burgwal, R. et al. Using an imperfect photonic network to implement random unitaries. *Opt. Express* **25**, 28236–28245 (2017).
53. Spagnolo, N. et al. General rules for bosonic bunching in multimode interferometers. *Phys. Rev. Lett.* **111**, 130503 (2013).
54. Aaronson, S. & Arkhipov, A. Bosonsampling is far from uniform. *Quantum Inf. Comput.* **14**, 1383–1423 (2014).
55. Spagnolo, N. et al. Experimental validation of photonic boson sampling. *Nat. Photonics* **8**, 615–620 (2014).
56. Carolan, J. et al. On the experimental verification of quantum complexity in linear optics. *Nat. Photonics* **8**, 621–626 (2014).
57. Crespi, A. et al. Suppression law of quantum states in a 3d photonic fast fourier transform chip. *Nat. Commun.* **7**, 10469 (2016).
58. Walschaers, M. et al. Statistical benchmark for BosonSampling. *N. J. Phys.* **18**, 032001 (2016).
59. Viggianiello, N. et al. Experimental generalized quantum suppression law in sylvester interferometers. *N. J. Phys.* **20**, 033017 (2018).
60. Agresti, I. et al. Pattern recognition techniques for boson sampling validation. *Phys. Rev. X* **9**, 011013 (2019).
61. Giordani, T. et al. Experimental statistical signature of many-body quantum interference. *Nat. Photonics* **12**, 173–178 (2018).
62. Flamini, F., Spagnolo, N. & Sciarino, F. Visual assessment of multi-photon interference. *Quantum Sci. Technol.* **4**, 024008 (2019).
63. Giordani, T. et al. Experimental quantification of four-photon indistinguishability. *N. J. Phys.* **22**, 043001 (2020).
64. Antón, C. et al. Interfacing scalable photonic platforms: solid-state based multi-photon interference in a reconfigurable glass chip. *Optica* **6**, 1471–1477 (2019).
65. Somaschi, N. et al. Near-optimal single-photon sources in the solid state. *Nat. Photonics* **10**, 340–345 (2016).
66. Wang, H. et al. Towards optimal single-photon sources from polarized microcavities. *Nat. Photonics* **13**, 770–775 (2019).
67. Atzeni, S. et al. Integrated sources of entangled photons at the telecom wavelength in femtosecond-laser-written circuits. *Optica* **5**, 311–314 (2018).
68. Youssry, A., Chapman, R. J., Peruzzo, A., Ferrie, C. & Tomamichel, M. Modeling and control of a reconfigurable photonic circuit using deep learning. *Quantum Sci. Technol.* **5**, 025001 (2020).
69. Skryabin, N. N., Dyakonov, I. V., Saygin, M. Y. & Kulik, S. P. Waveguide-lattice-based architecture for multichannel optical transformations. *Opt. Express* **29**, 26058–26067 (2021).
70. Jahangiri, S., Arrazola, J. M., Quesada, N. & Killoran, N. Point processes with gaussian boson sampling. *Phys. Rev. E* **101**, 022134 (2020).
71. Arrazola, J. M., Bromley, T. R. & Reberntrost, P. Quantum approximate optimization with gaussian boson sampling. *Phys. Rev. A* **98**, 012322 (2018).
72. Corrielli, G. et al. Symmetric polarization-insensitive directional couplers fabricated by femtosecond laser writing. *Opt. Express* **26**, 15101 (2018).
73. Ceccarelli, F., Atzeni, S., Principe, A., Farinano, R. & Osellame, R. Thermal Phase Shifters for Femtosecond Laser Written Photonic Integrated Circuits. *J. Light Technol.* **37**, 4275–4281 (2019).

ACKNOWLEDGEMENTS

This work is supported by the European Union's Horizon 2020 research and innovation program through the FET project PHOQUISING ("PHOTonic Quantum SAMPLING machine" - Grant Agreement No. 899544) and under the ERC project CAPABLE ("Composite integrATed Photonic pLATFORM By ultrafast LasEr micromachining" - Grant Agreement No. 742745). The authors wish to acknowledge financial support also by MIUR (Ministero dell'Istruzione, dell'Università e della Ricerca) via project PRIN 2017 "Taming complexity via Quantum Strategies: a Hybrid Integrated Photonic approach" (QUSHIP - Id. 2017SRNBRK). Z.-N. T. acknowledges funding by Quantero programme (project HiPhoP - High-dimensional quantum Photonic Platform; grant agreement no. 731473). Fabrication of the device was partially performed at PoliFAB, the micro- and nanofabrication facility of Politecnico di Milano (<https://www.polifab.polimi.it>). The authors would like to thank the PoliFAB staff for valuable technical support.

AUTHOR CONTRIBUTIONS

F.H. and S.P. contributed equally to this work. F.H., T.G., G.C., N.S., F.S., S.P., A.Cr., and R.O. conceived the experiment. S.P., Z.-N.T., F.C., A.Cr., and R.O. fabricated and characterized the integrated device using classical optics. F.H., T.G., M.I., C.E., A.Ca., G.C., N.S., and F.S. carried out the quantum experiments and performed the data analysis. All the authors discussed the results and contributed to the writing of the paper.

COMPETING INTERESTS

The authors declare no competing interests.

ADDITIONAL INFORMATION

Supplementary information The online version contains supplementary material available at <https://doi.org/10.1038/s41534-022-00568-6>.

Correspondence and requests for materials should be addressed to Fabio Sciarino or Roberto Osellame.

Reprints and permission information is available at <http://www.nature.com/reprints>

Publisher's note Springer Nature remains neutral with regard to jurisdictional claims in published maps and institutional affiliations.



Open Access This article is licensed under a Creative Commons Attribution 4.0 International License, which permits use, sharing, adaptation, distribution and reproduction in any medium or format, as long as you give appropriate credit to the original author(s) and the source, provide a link to the Creative Commons license, and indicate if changes were made. The images or other third party material in this article are included in the article's Creative Commons license, unless indicated otherwise in a credit line to the material. If material is not included in the article's Creative Commons license and your intended use is not permitted by statutory regulation or exceeds the permitted use, you will need to obtain permission directly from the copyright holder. To view a copy of this license, visit <http://creativecommons.org/licenses/by/4.0/>.

© The Author(s) 2022